

pubs.acs.org/NanoLett Letter

# Morphologic Design of Silver-Bearing Sugar-Based Polymer Nanoparticles for Uroepithelial Cell Binding and Antimicrobial Delivery

Yue Song, Mahmoud Elsabahy, Christina A. Collins, Sarosh Khan, Richen Li, Teri N. Hreha, Yidan Shen, Yen-Nan Lin, Rachel A. Letteri, Lu Su, Mei Dong, Fuwu Zhang, David A. Hunstad,\* and Karen L. Wooley\*



Cite This: Nano Lett. 2021, 21, 4990-4998



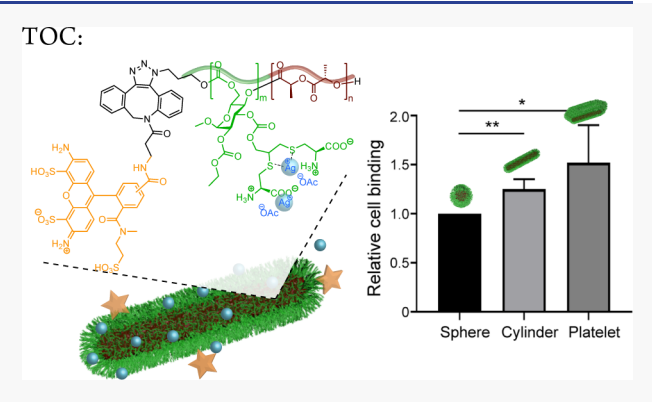
ACCESS

III Metrics & More

Article Recommendations

s Supporting Information

ABSTRACT: Platelet-like and cylindrical nanostructures from sugarbased polymers are designed to mimic the aspect ratio of bacteria and achieve uroepithelial cell binding and internalization, thereby improving their potential for local treatment of recurrent urinary tract infections. Polymer nanostructures, derived from amphiphilic block polymers composed of zwitterionic poly(D-glucose carbonate) and semicrystalline poly(L-lactide) segments, were constructed with morphologies that could be tuned to enhance uroepithelial cell binding. These nanoparticles exhibited negligible cytotoxicity, immunotoxicity, and cytokine adsorption, while also offering substantial silver cation loading capacity, extended release, and *in vitro* antimicrobial activity (as effective as free silver cations) against uropathogenic *Escherichia coli*. In comparison to spherical analogues,



cylindrical and platelet-like nanostructures engaged in significantly higher association with uroepithelial cells, as measured by flow cytometry; despite their larger size, platelet-like nanostructures maintained the capacity for cell internalization. This work establishes initial evidence of degradable platelet-shaped nanostructures as versatile therapeutic carriers for treatment of epithelial infections.

**KEYWORDS:** Silver-bearing polymer nanostructures, antimicrobial, cell-binding and internalization, platelet-shaped nanostructures, urinary tract infections

## INTRODUCTION

Urinary tract infections (UTIs) are among the most common bacterial infections acquired in the community and in hospitals, <sup>1,2</sup> and recurrent UTIs can arise from re-emergence of bacterial colonies that are impervious to standard antibiotic treatment while they persist within epithelial cells lining the urinary bladder.<sup>3,4</sup> Globally, increasing antibiotic resistance among uropathogens further makes these recalcitrant UTIs challenging to treat.<sup>5–7</sup> Alternative strategies utilize biocides with low likelihood of resistance development; for example, silver cations (Ag<sup>+</sup>), the predominant antimicrobial silver species, exert activity against a broad spectrum of bacteria and other microbes and rarely elicit bacterial resistance.<sup>8–12</sup>

For intracellular delivery of therapeutics, polymer nanocarriers offer capacity for encapsulating various antimicrobial agents and for optimizing nanoparticle (NP) cell binding and uptake, by installing targeting ligands or modulating NP physical and mechanical properties (e.g., size, shape, chemical composition, surface chemistry, and modulus). 12-18 It is hypothesized that adherence and internalization of *E. coli* within epithelial cells is facilitated by multivalent adhesinreceptor binding interactions and by the elongated rod-like aspect ratio of these Gram-negative bacilli, <sup>3,19</sup> features that can both be leveraged in the chemical design of nanocarriers. Previous work demonstrated that shell cross-linked knedel-like (SCK) spherical NPs having dimensions of *ca.* 20–40 nm and functionalized with *E. coli* FimH<sub>A</sub>, the type 1 pilus tip adhesin that mediates bacterial attachment to bladder epithelium, <sup>20</sup> readily bound cultured uroepithelial cells but were rarely internalized. <sup>21,22</sup> This result indicated that, despite specific interactions between NPs and cell-surface receptors, achieving epithelial internalization of NPs would require more than merely installing a targeting ligand. A logical next approach relies on the optimization of NP size and shape to promote multivalent cell binding and improve internalization. <sup>23,24</sup>

Received: February 23, 2021 Revised: May 24, 2021 Published: June 11, 2021





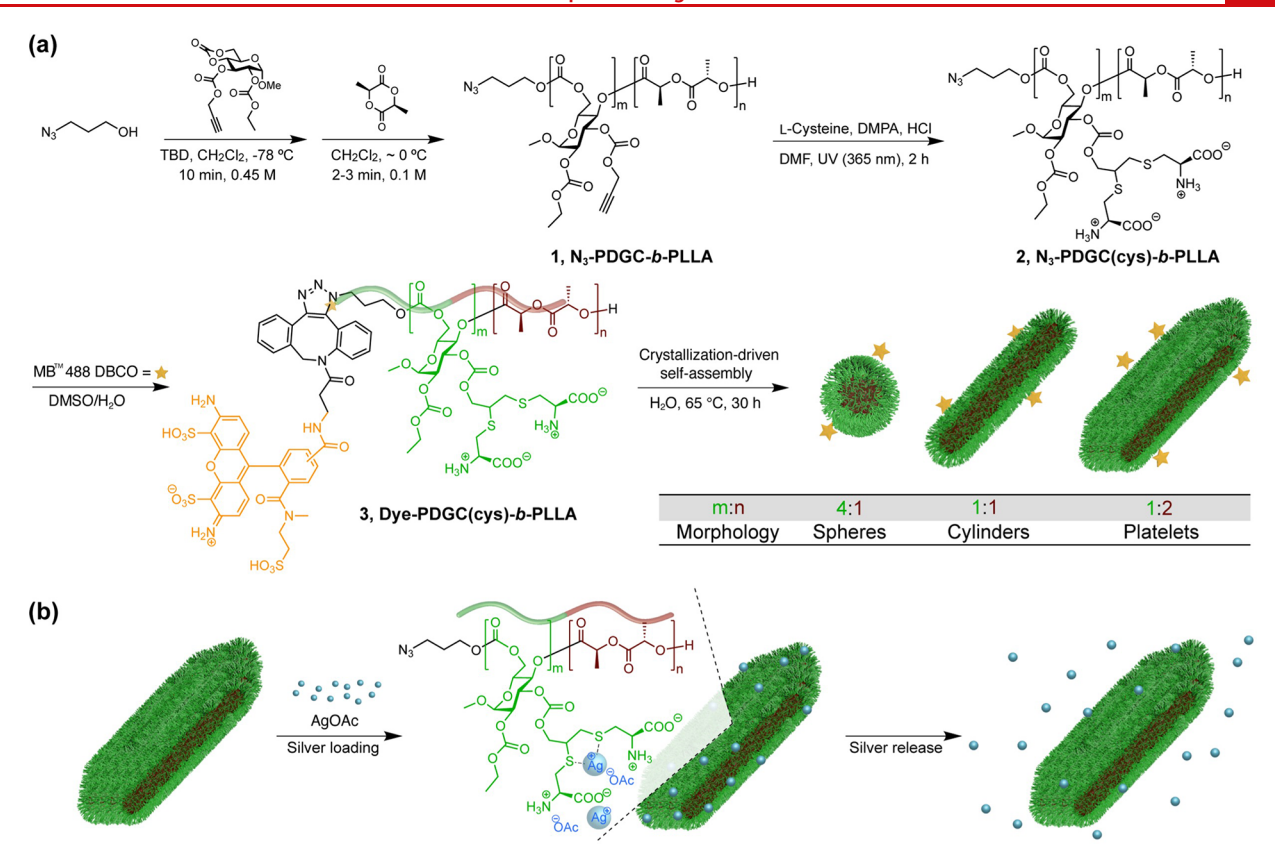


Figure 1. Synthetic schemes. (a) Synthesis of polymer 1, N<sub>3</sub>-PDGC-*b*-PLLA, by ROP of glucose-carbonate and L-lactide monomers with an azido-containing initiator, followed by postpolymerization modification via thiol—yne reaction with cysteine to prepare the zwitterionic polymer 2, N<sub>3</sub>-PDGC(cys)-*b*-PLLA, and chain-end modification of polymer 2 with DBCO-functionalized fluorescent dye to afford dye-labeled polymer 3, dye-PDGC(cys)-*b*-PLLA. (b) AgOAc loading into polymer nanostructures, through interactions with dithioether and carboxylate groups, and release.

Due in part to their anisotropic properties, rod-like NPs have attracted growing interest. 25,26 Gratton et al. reported rapid and efficient internalization of rod-like, high-aspect-ratio hydrogel particles with dimensions as large as 3  $\mu$ m by human cervical carcinoma epithelial (HeLa) cells.<sup>27</sup> Liu et al. elucidated the effect of the aspect ratio of rod-like NPs on cellular uptake, showing that rods with aspect ratios of 4 and 8 were internalized faster by both epithelial and endothelial cells than rods with an aspect ratio of 17.28 Further, Agarwal et al. revealed that uptake of disc-shaped hydrophilic NPs into cultured mammalian cells was more efficient than for nanorods made from similar materials.<sup>29</sup> Additionally, Decuzzi et al. have shown, theoretically, that nonspherical oblate-shaped particles bind more strongly and can withstand higher linear shear-flow forces than spherical NPs,<sup>30</sup> a consideration important in designing NPs for urinary tract use. These observations highlight the importance of NP morphology and dimension in creating optimized therapeutic carriers.

Here, we report the design of multifunctional, fully degradable synthetic zwitterionic block copolymers to afford micellar nanostructures of spherical, cylindrical, and platelet-like morphologies, and we evaluate the effect of NP morphology and dimension on cellular binding and internalization. Biocompatibility of these nanocarriers was evaluated by measurement of cell viabilities and cytokine expression levels. Platelet-like and cylindrical nanostructures displayed greater cell binding and internalization properties, compared to spherical NPs. Finally, loading capacity and release kinetics of antimicrobial silver cations were quantified, and the *in vitro* 

antimicrobial activities of silver-loaded NPs against pathogenic bacteria were determined.

## ■ RESULTS AND DISCUSSION

Design of Multifunctional Polymeric Nanocarriers with Varied Morphology. To construct nanocarriers of varied morphology from biobased amphiphilic block polymers, synthetic building blocks were designed with tunable backbone chemical compositions and functional diversity rendered by side-chain and chain-end groups. Semicrystalline poly(Llactide) (PLLA) was used as the hydrophobic segment due to its excellent performance in crystallization-driven selfassembly (CDSA), which facilitated formation of high-aspectratio NPs.<sup>31</sup> Zwitterionic cysteine-modified poly(D-glucose carbonate) (PDGC)<sup>32</sup> served as the hydrophilic segment, chosen for its naturally derived cysteine and glucose building blocks, versatile functionality, and degradability into environmentally benign molecules, 33,34 potentially increasing biocompatibility and minimizing toxicity.<sup>35</sup> Zwitterions were introduced to the PDGC block for hydrophilicity and biocompatibility and to enable antimicrobial metal chelation. In this study, the functional and degradable diblock copolymer N<sub>3</sub>-PDGC(cys)-b-PLLA was designed to incorporate the features of a zwitterionic hydrophilic shell, semicrystalline hydrophobic core, and specially installed chain-end azido group for fluorescent labeling (Figure 1a). A series of fluorescently labeled amphiphilic diblock copolymers having similar overall degrees of polymerization yet different hydrophilic-to-hydrophobic ratios was readily prepared in three steps

per each block polymer, from an azide-functionalized alcohol initiator, an alkyne-functionalized cyclic glucose carbonate monomer, L-lactide comonomer, cysteine, and MB 488 dibenzocyclooctyne (DBCO). These polymers were then assembled into nanocarriers, and the effects of NP morphology on epithelial cell binding and internalization were investigated. Subsequently, NPs were loaded with silver cations and studied for their ability to inhibit *E. coli* growth.

Synthesis and Modification of Multifunctional Amphiphilic Copolymers. The diblock copolymers were synthesized through sequential controlled ring-opening polymerizations (ROP)<sup>34,36-38</sup> of alkyne-functionalized cyclic Dglucose carbonate, followed by L-lactide. 3-Azido-1-propanol was utilized as the initiator to afford diblock copolymers with an azido group at the polymer  $\alpha$ -chain end, capable of chemical conjugation of a fluorescent dye or targeting ligand. Of note, the monomer addition order is important to place the reactive azido group at the hydrophilic end of the chain to avail it for use in micelle surface functionalization. In a one-pot sequential ROP process, the cyclic carbonate of glucose was allowed to undergo polymerization at -78 °C in dichloromethane for 10 min, followed by removal of the reaction mixture from the dry ice/acetone bath and the introduction of L-lactide and additional dichloromethane, with the polymerization being allowed to proceed for an additional 2-3 min before being quenched by the addition of acetic acid. Allowing the temperature to increase from -78 °C to ca. 0 °C and decreasing the concentration of the reaction mixture from 0.45 to 0.1 M for polymerization of the second L-lactide block were important to maintain the narrow dispersity of the polymer, likely because the reduced viscosity of the reaction mixture promoted better PLLA chain extension. Informed by our prior work,<sup>32</sup> we designed three different PDGC-to-PLLA ratios (4:1, 1:1, and 1:2) of polymer 1, N<sub>3</sub>-PDGC-b-PLLA, to achieve spherical, cylindrical, and platelet-like nanostructure morphologies, respectively. Size-exclusion chromatography (SEC) revealed unimodal molar mass distributions and low dispersities, demonstrating well-defined structures of the diblock copolymers (Table S1, Figure S1). After purification of the polymers by precipitation into methanol, the degree of polymerization  $(DP_n)$  of each block was determined from  ${}^{1}H$ NMR spectroscopy (Figures S2 and S3) by comparing the integration of the initiator N<sub>3</sub>CH<sub>2</sub>CH<sub>2</sub>CH<sub>2</sub>O central methylene proton resonance (1.95 ppm) with the integrations of the resonances of protons attached to the glucose anomeric carbons (5.03 ppm) in the PDGC segment and methine protons (5.16 ppm) from the PLLA segment, and the molar mass  $(M_n)$  values were then calculated. For the series of three polymer 1 samples, the DP<sub>n</sub> values of PDGC vs PLLA, m:n, were determined to be 70:18, 47:44, and 39:74, providing the desired 4:1, 1:1, and 1:2 proportions of PDGC-to-PLLA. Fourier transform infrared (FT-IR) spectroscopy confirmed the presence of the azide functional group, by an azide stretching band observed at 2106 cm<sup>-1</sup> (Figure S4).

The three polymers 1 were then modified via a photo-initiated thiol—yne click reaction with cysteine (10 equiv to alkyne groups) under UV light (365 nm) in the presence of 2,2-dimethoxy-2-phenylacetophenone (DMPA) for 2 h, to facilitate quantitative conversion of the alkyne functional groups on the polymers and minimize polymer cross-linking. Dialysis against nanopure water (pH 3, adjusted with HCl) at 4 °C and lyophilization were performed to afford the series of three amphiphilic block copolymers 2 as white powders. The

appearance of thioether proton resonances at 3.06 and 3.31 ppm and the disappearance of the alkyne proton signal resonating at 3.57 ppm (Figures S5 and S6) indicated successful conjugation of cysteine side-chain substituents. FT-IR spectroscopy further supported the introduction of COO-H and N-H groups by showing a broad peak at 3600-2300 cm<sup>-1</sup> (Figure S7), while indicating the carboxylate (COO-) characteristic of cysteine with a peak attributed to carboxylate C=O stretching at 1627 cm<sup>-1</sup> (Figure S8). Thermogravimetric analysis (TGA) of polymer 2 revealed twostage decomposition with different extents of mass loss for the different m:n values, but an overall trend of 10-20% mass loss at 160-190 °C and 30-50% mass loss at 220-320 °C (Figure S9), corresponding to the loss of cysteine moieties and decomposition of the polymer backbone, respectively, with ca. 20% mass remaining at 500 °C.

The dye-functionalized polymers 3 were obtained by copper-free strain-promoted azide-alkyne cycloaddition of MB 488 DBCO with the azido group at the polymer chain end. Polymer 2 and fluorescent dye MB 488 DBCO were allowed to undergo reaction in a mixture of DMSO and H<sub>2</sub>O (10:1) at room temperature, while wrapped with aluminum foil to avoid potential photobleaching. This chemistry would enable facile decoration of polymers 2 with dyes without UV irradiation, heat, or applying metal catalysts, 39,40 thereby reducing potential toxicity in traditional copper-catalyzed azide-alkyne cycloaddition, minimizing fluorescence quenching, and improving the cycloaddition reactivity. The appearance of resonances attributed to DBCO and dye protons in the aromatic region of 8.28-6.95 ppm indicated successful dyepolymer conjugation (Figure S10). Diffusion-ordered spectroscopic (DOSY-NMR) analysis of polymer 3 samples provided further evidence of the successful dye-polymer conjugation by showing the same diffusion coefficient of the chain-end dye and polymer backbone protons at ca.  $5 \times 10^{-11}$  m<sup>2</sup>/s, whereas free dye molecules in the presence of polymer (nonreactive chain end) displayed a different diffusion coefficient at ca. 4 × 10<sup>-10</sup> m<sup>2</sup>/s (Figure S11). UV-vis spectroscopy revealed a maximum absorption at 498 nm, and spectrophotometry of the dye-polymer conjugate showed an excitation maximum at 501 nm and emission maximum at 528 nm (Figure S12).

Crystallization-Driven Self-Assembly (CDSA) into Nanostructures with Varied Morphology. Self-assembly of the three polymer 3 samples was performed through CDSA, 41-45 following previously described procedures, 32 to afford nanostructures of varied morphologies. Briefly, dispersions of dye-PDGC(cys)-b-PLLA in nanopure water (0.05-0.1 mg/mL) were allowed to undergo vortex, sonication, and then incubation at 65 °C for 30 h, followed by cooling to room temperature. Transmission electron microscopy (TEM) analysis (Figure 2) of polymer 3 with a hydrophilic-to-hydrophobic DP ratio at 70:18, 47:44, and 39:74 showed spheres ( $D_{av} = 11 \pm 2 \text{ nm}$ ), cylinders ( $L_{av} = 220$  $\pm$  66 nm,  $D_{av} = 17 \pm 4$  nm), and platelet-like nanostructures  $(L_{av} = 620 \pm 110 \text{ nm}, W_{av} = 160 \pm 35 \text{ nm})$ , respectively. Polymers with the lowest PLLA content (ca. 6 wt %) yielded spherical micelles with measured diameters (D) of 6-14 nm. Elongated cylindrical nanostructures were obtained from polymers having PLLA contents of ca. 18 wt %, while the platelet-like nanostructures were formed by polymers with PLLA reaching ca. 30 wt % (1:2, PDGC:PLLA, m = 39, n =74). The cylindrical micelles had measured length (L) values from 150-350 nm, with D values of 13-24 nm. Platelet-like

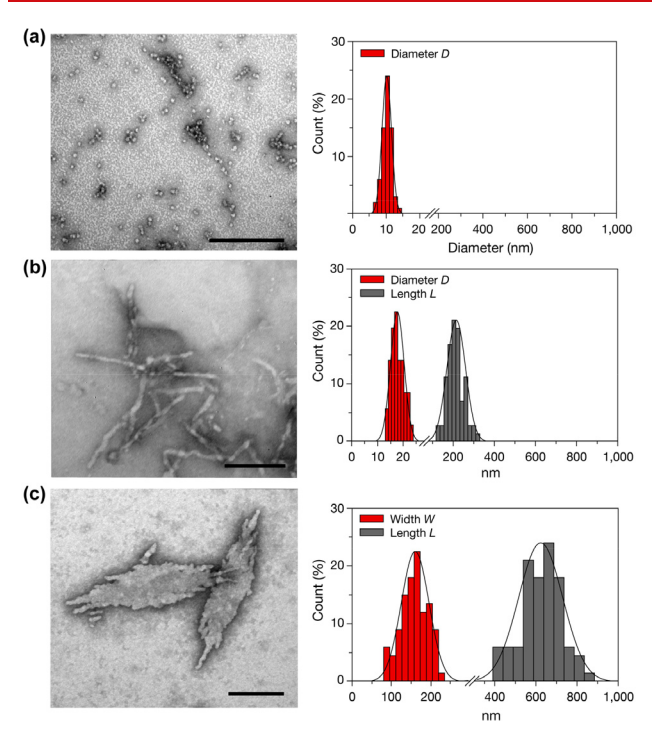


**Figure 2.** Morphology characterization of nanostructures. TEM images (left) and histograms of the diameter/contour length/width distributions determined from measurement of *ca.* 50 particles (right) of the nanostructures assembled from dye-containing block copolymers (a) dye-PDGC(cys)<sub>70</sub>-b-PLLA<sub>18</sub>, (b) dye-PDGC(cys)<sub>47</sub>-b-PLLA<sub>44</sub>, and (c) dye-PDGC(cys)<sub>39</sub>-b-PLLA<sub>74</sub> (scale bar, 200 nm).

nanostructures (L = 400-900 nm) were found to be significantly longer than cylinders and exhibited widths (W) of 80–230 nm, revealing not only a morphologic aspect ratio

difference but also significant size differences between the cylinders and platelets. Additionally, only a small quantity of spherical nanoparticles was observed in cylinder and platelet samples by TEM (Figure S13), indicating generally narrow-dispersed nanoparticle morphology within each sample, beneficial for studying the effects of morphology and size on performance. In total, these results demonstrated the feasibility of accessing diverse nanostructure morphologies of polymer 3 to enable investigation of the nanostructure shape and dimension effects on uroepithelial binding and internalization.

Bladder Epithelial Cell Binding and Internalization. Flow cytometry and fluorescent confocal microscopy characterizations were carried out on the fluorescently labeled NPs derived from dye-PDGC(cys)<sub>70</sub>-b-PLLA<sub>18</sub>, dye-PDGC(cys)<sub>47</sub>b-PLLA<sub>44</sub>, and dye-PDGC(cys)<sub>39</sub>-b-PLLA<sub>74</sub> to quantitatively determine their association with uroepithelial cells and visualize internalization, respectively. Cultured uroepithelial cells, either as subconfluent adherent cells or in suspension, were treated with MB 488-labeled NPs of various morphologies, using concentrations and exposure times established in our prior work.<sup>21</sup> Cellular association with NPs was quantified by flow cytometry, and internalization was observed qualitatively by confocal fluorescence microscopy after cellsurface staining with AlexaFluor 594-labeled wheat germ agglutinin (WGA). Shape-dependent differences in uroepithelial binding were observed using dilute (25  $\mu$ g/mL polymer) suspensions of NPs. Specifically, NPs with the platelet or cylinder morphology exhibited higher binding than spheres (Figure 3a,b). Furthermore, 3D-reconstructed z-stacks of confocal images were used to localize intracellular NPs. This analysis visually confirmed more cell association by platelet NPs (Figure 3c), though precise quantification of internalized NPs was not possible with this method. Taken together, our results suggested that the enlarged and elongated dimensions

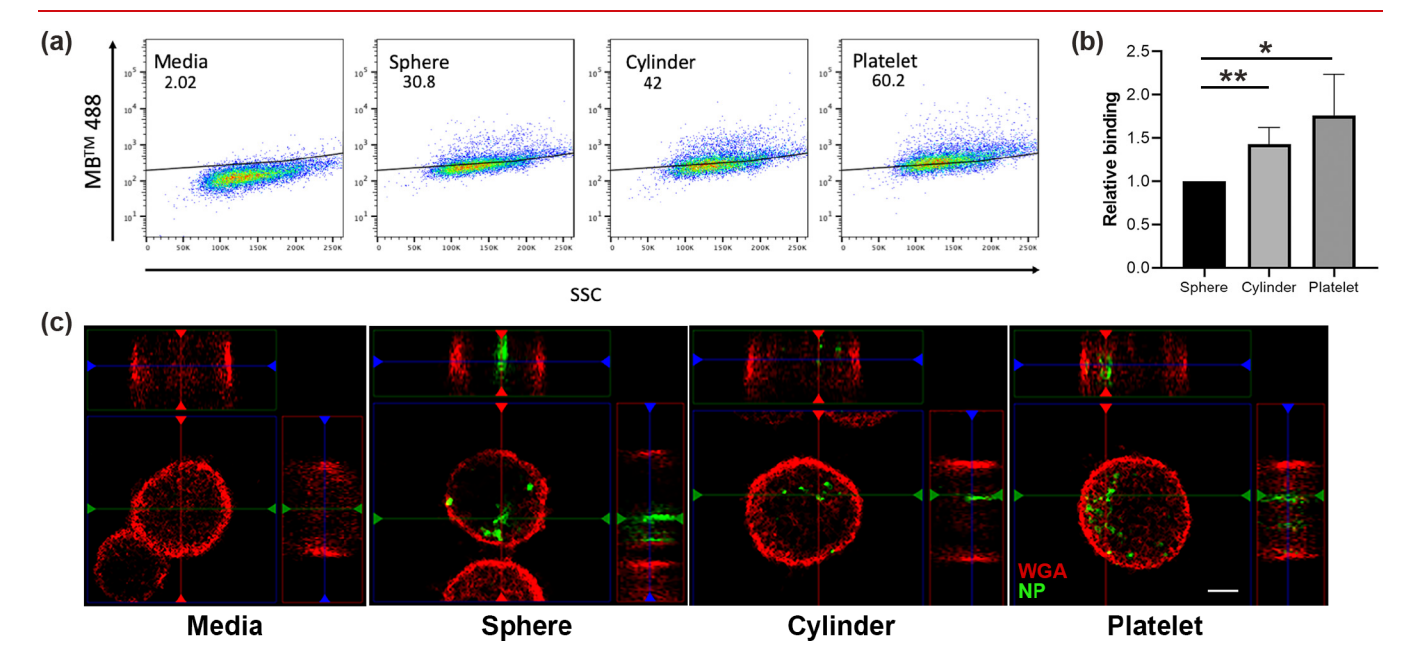


Figure 3. Assessment of cell binding and uptake of NPs. (a) Flow cytometric analysis of cultured uroepithelial cells inoculated with MB 488-labeled PDGC(cys)-b-PLLA NPs having sphere, cylinder, or platelet morphologies. The proportions of cells bearing bound and internalized NPs (over four experiments) were sphere,  $36.2\% \pm 6.5\%$ ; cylinder,  $49.5\% \pm 10.3\%$ ; and platelet,  $58.4\% \pm 15.6\%$ . Representative flow plots from one experiment shown. (b) Binding efficiencies of NPs expressed with sphere set to "1" as the reference condition; the cylinder and platelet were each statistically greater than the sphere (\*P < 0.05 and \*\*P < 0.01 by t test). (c) Confocal microscopy images with orthogonal projections showing multiple dye-labeled NPs internalized within uroepithelial cells (surfaces labeled with WGA 594); scale bar,  $5~\mu$ m (all panels).

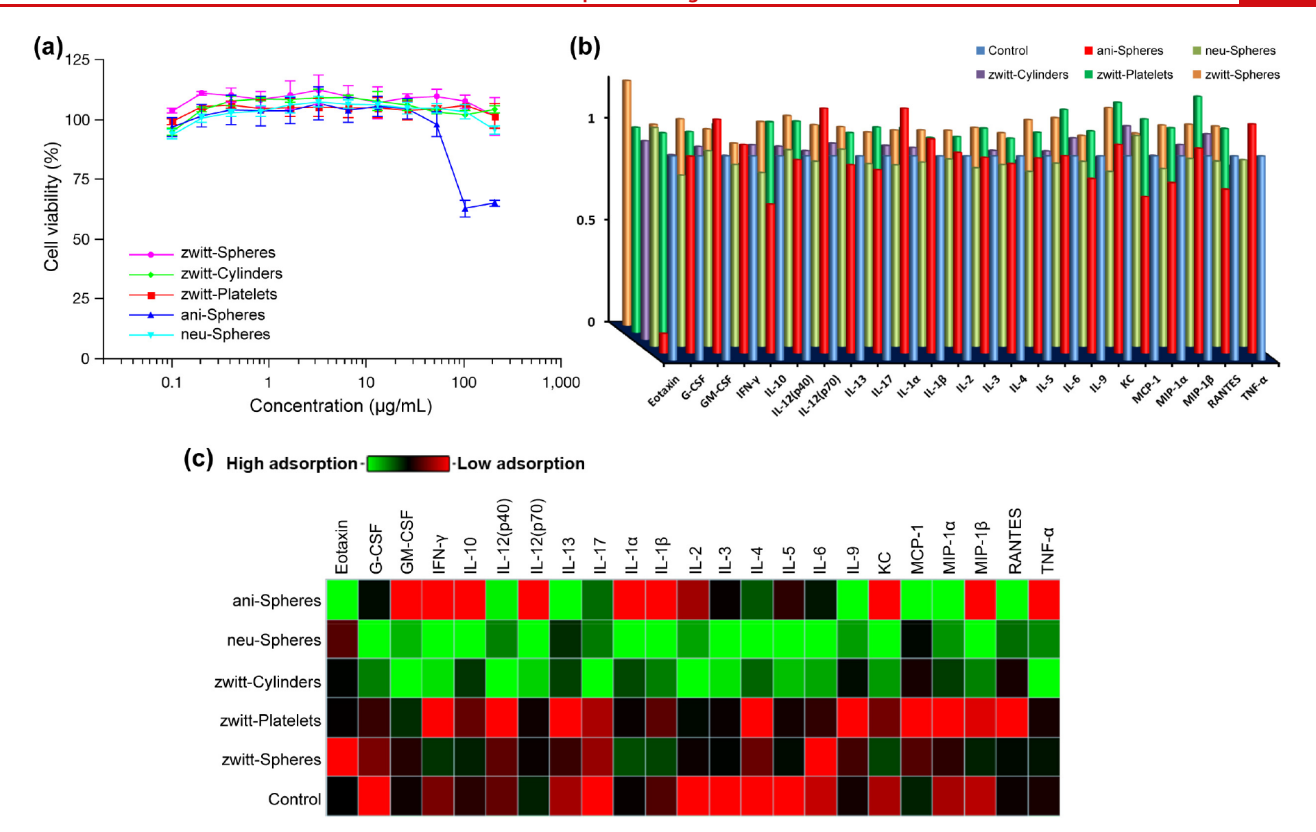


Figure 4. Cytotoxicity, immunotoxicity, and cytokine adsorption assessments of zwitterionic nanostructures of different morphologies, in comparison with anionic (ani-spheres) and neutral (neu-spheres) polymer nanoparticles. (a) Uroepithelial cell viabilities after treatment with polymer nanoparticles at concentrations ranging from 1.5 to 210  $\mu$ g/mL for 72 h (triplicate experiments). (b) Cytokine adsorption of different polymer nanoparticles was assessed by measuring the concentration of cytokines in supernatants after incubation of RAW cells, as compared to untreated samples. (c) Heat map for the cytokine adsorption assay showing the relative concentrations of various cytokines after incubation of cytokine standards with different polymer NPs (control is cytokine standards without nanoparticles).

offered by the platelet and spherical morphologies confer improved binding compared with spheres, favoring uroepithelial internalization despite their larger overall size.

Evaluation of Nanostructure Toxicity. The affinity of polymer nanostructures to the epithelial cell surface could be mediated by interactions between nanostructure corona and cell-surface proteins. We therefore investigated their potential cytotoxicity, immunotoxicity, and cytokine adsorption activity, which are essential factors to consider for the development of materials in biomedical applications (Figure 4). To gain further understanding of the effect of nanostructure morphology and whether their specific zwitterionic surface characteristics are beneficial in mitigating the nanostructure toxicity, measurements of zwitterionic NPs were compared with anionic (carboxylic acid-functionalized N<sub>3</sub>-PDGC(COOH)-b-PLLA) and neutral (PEG-functionalized N<sub>3</sub>-PDGC(PEG)-b-PLLA) spherical nanoparticles (Figure S14). In vitro cytotoxicity was appraised by incubating nanostructures of different morphologies and surface chemistries with cultured uroepithelial cells (5637; ATCC HTB-9). The three different morphologic zwitterionic NPs, as well as neutral spherical NPs, exhibited no observable cytotoxicity to uroepithelial cells over the tested concentration range (1.5–210  $\mu$ g/mL, Figure 4a), supporting the biocompatibility of these core-shell nanostructured polymeric micelles. In comparison, anionic NPs caused a reduction in cell viability at concentrations > 60  $\mu$ g/mL, consistent with previous results.46 Immunotoxicity was evaluated by incubating RAW 264.7 mouse macrophages with various NP formulations for 24 h and then measuring the

expression levels of 23 cytokines using a multiplex assay. 47 No significant overexpression of any of the tested cytokines was observed when compared to untreated cells (Figure 4b). Independently, the cytokine adsorption assay was performed by measuring the levels of 23 cytokine standards when premixed with polymer NPs of different morphologies and different surface chemistries (Figure 4c), in comparison to the same biomarker concentrations in the absence of the test materials. This experiment was conducted for two purposes. First, cytokines may be adsorbed on surfaces and/or within internal regions of NPs, thereby generating inaccurately low measurements of the immunotoxic effect. 47,48 Second, the adsorption assay provides an indication of the adsorption of biomolecules (biofouling) onto the NPs. Spherical zwitterionic NPs showed much lower adsorption of cytokines compared to anionic and neutral NPs of the same spherical morphology (Figure 4c). Among zwitterionic NPs of three morphologies, the least adsorption of the measured cytokines was observed with platelet-like NPs, while the highest adsorption was observed for the zwitterionic cylindrical NPs. These results demonstrated that zwitterionic nanostructures have favorable antibiofouling properties, supporting their viability as nanocarriers for biomedical delivery applications. 49,50 Further studies may illuminate the variations observed in cytokine adsorption with different zwitterionic NP morphologies.

Preparation of Silver-Loaded Nanostructures, Silver Release Kinetics, and Antibacterial Activity. Silver cations were chosen as antibacterial cargo for their chemical compatibility, low propensity to elicit resistance, <sup>51</sup> and biocidal

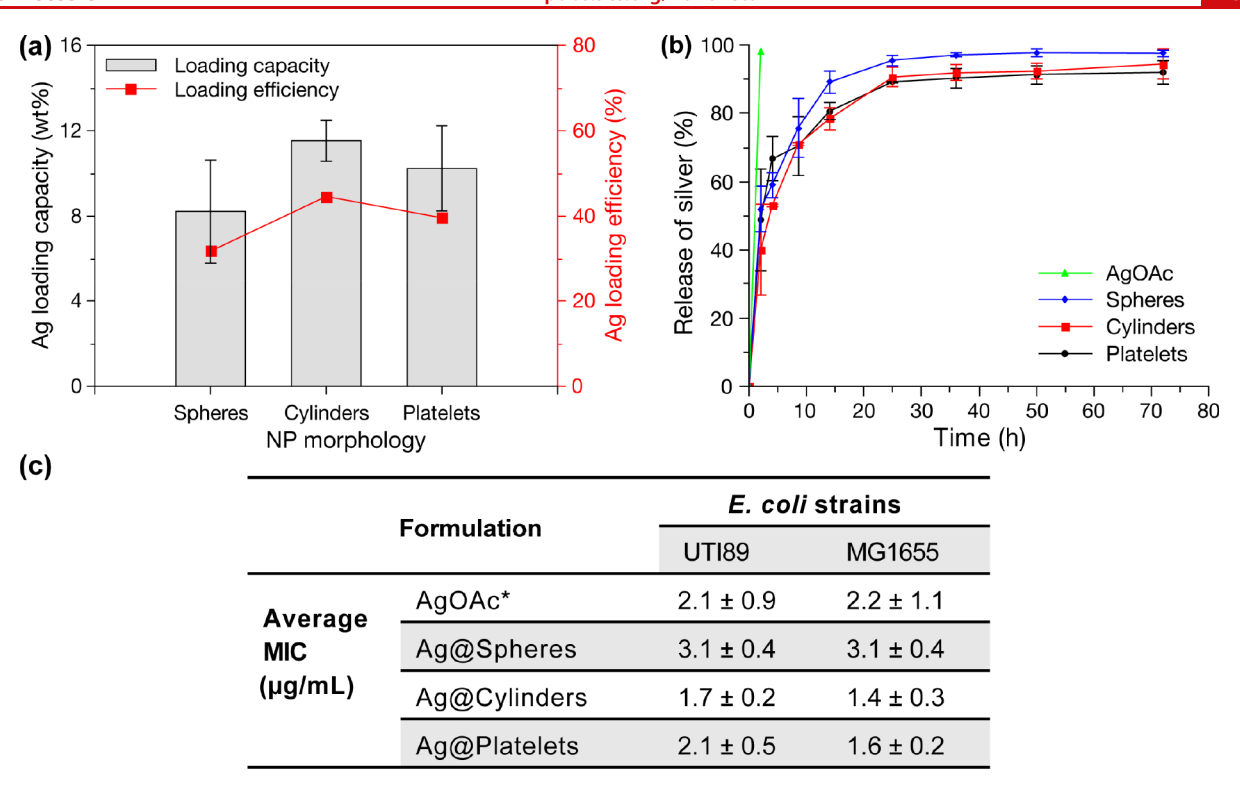


Figure 5. Silver loading, release, and antimicrobial activity in nanostructures. (a) Silver-loading capacities (wt %, left axis; bars) and efficiencies (%, right axis; lines and symbols) of AgOAc with 40 wt % AgOAc feed. (b) Release profiles of silver from dialysis cassettes containing solutions of silver-loaded NPs at 37 °C in phosphate buffer with 10 mM NaCl. Average values were calculated from triplicate experiments; error bars indicate the standard error of the mean. (c) MICs ( $\mu$ g/mL Ag $^+$ ) of silver acetate and silver-bearing NPs (Ag@spheres, Ag@cylinders, and Ag@platelets), against *E. coli* strains; \*AgOAc MIC values from a prior study<sup>52</sup> are shown for comparison.

activity that does not require active bacterial replication or macromolecular synthesis. Encapsulation of silver into zwitterionic nanoparticles was achieved using silver acetate (40 wt %) via interactions with the cysteine carboxylate groups and dithioether moieties within the hydrophilic nanostructure corona (Figure 1b). Total Ag loadings were 8–12 wt % and were generally independent of NP morphology, as determined by inductively coupled plasma mass spectrometry (ICP-MS) (Figure 5a). TEM revealed that the nanostructures retained their original morphologies after encapsulation of Ag (Figure S15), likely due to the existence of the semicrystalline PLLA core of the nanostructures.<sup>32</sup>

Release of Ag from the nanostructures was determined by monitoring the decrease of [Ag] inside dialysis cassettes against 10 mM phosphate buffer with 10 mM NaCl (pH 7.4) at 37 °C, quantified by ICP-MS (Figure 5b). As expected, compared to free unbound AgOAc, it was found that these zwitterionic nanostructures liberated silver in a sustained manner, with a release half-life  $(t_{1/2})$  of 3–5 h. Furthermore, packaged silver cations were stable in aqueous solution for more than a week without visible precipitation, thus displaying the colloidal stability needed for *in vitro* and *in vivo* applications. The release characteristics of these antimicrobial nanotherapeutics may be beneficial during local administration (i.e., direct epithelial treatment).

The antimicrobial activity of Ag-loaded NPs was examined by measurement of minimum inhibitory concentrations (MICs) against two strains of *E. coli* (uropathogenic strain UTI89 and laboratory strain MG1655). The MICs of the silver-bearing NPs, expressed as  $\mu$ g/mL of Ag<sup>+</sup>, were compared with silver acetate (Figure 5c, averaged from n = 7 replicates).

The silver-loaded NPs showed similar potencies against UTI89 and MG1655 as free silver acetate, with MICs  $\leq 3.1~\mu g/mL$ , which were comparable to the values measured with earlier silver-bearing constructs (1–4  $\mu g/mL$  Ag<sup>+</sup>). These antibacterial activities against *E. coli* indicated that the incorporated silver is readily available for antimicrobial activity and demonstrated the suitability of using polymer nanostructure platforms for silver-based antimicrobial delivery.

# CONCLUSIONS

In summary, we have developed multifunctional polymer nanocarriers assembled from zwitterionic amphiphilic block copolymers to probe, fundamentally, the roles of nanostructure size, shape, and morphology on their interactions with and responses by biological systems. These constructs exhibit high biocompatibility and morphology-dependent epithelial cell binding and internalization and can be loaded with silver antimicrobials, thereby providing strategies to combat recurrent urinary tract infections. Natural product-based amphiphilic diblock copolymers of different hydrophilic-tohydrophobic ratios were synthesized by sequential ROPs; orthogonal "click" modifications introduced zwitterionic hydrophilic moieties along the side chain and fluorescent dyes at the  $\alpha$ -chain end. Well-defined nanostructures with tunable size and morphology (spheres, cylinders, and platelets) were prepared via CDSA. The cylindrical and platelet morphologies exhibited the highest uroepithelial binding, and internalization was most evident with platelet NPs. Cyto- and immunotoxicities were negligible. When loaded with silver cation antimicrobials, sustained release profiles were obtained, and growth of two E. coli strains was inhibited, confirming the

availability of the incorporated silver for antimicrobial activity with potency comparable to free Ag<sup>+</sup>. The building blocks used here yielded functional nanomaterials with therapeutic potential and the ability to degrade into bioresorbable components. We further demonstrate the importance of morphology, in addition to composition, in optimizing nanocarrier design for the epithelial delivery of therapeutic cargo.

## ASSOCIATED CONTENT

## Supporting Information

The Supporting Information is available free of charge at https://pubs.acs.org/doi/10.1021/acs.nanolett.1c00776.

Experimental procedures and additional <sup>1</sup>H NMR, DOSY NMR, FT-IR, TGA, and TEM results (PDF)

#### AUTHOR INFORMATION

## **Corresponding Authors**

David A. Hunstad — Department of Pediatrics and Department of Molecular Microbiology, Washington University School of Medicine, St. Louis, Missouri 63110, United States; Email: dhunstad@wustl.edu

Karen L. Wooley — Department of Chemistry, Texas A&M University, College Station, Texas 77842, United States; orcid.org/0000-0003-4086-384X; Email: wooley@chem.tamu.edu

#### **Authors**

Yue Song — Department of Chemistry, Texas A&M University, College Station, Texas 77842, United States; orcid.org/0000-0002-7800-5528

Mahmoud Elsabahy — Science Academy, Badr University in Cairo, Badr City, Cairo 11829, Egypt; Department of Chemistry, Texas A&M University, College Station, Texas 77842, United States; © orcid.org/0000-0003-3341-1829

Christina A. Collins – Department of Pediatrics, Washington University School of Medicine, St. Louis, Missouri 63110, United States

Sarosh Khan – Department of Chemistry, Texas A&M University, College Station, Texas 77842, United States

Richen Li – Department of Chemistry, Texas A&M University, College Station, Texas 77842, United States

Teri N. Hreha – Department of Pediatrics, Washington University School of Medicine, St. Louis, Missouri 63110, United States

Yidan Shen — Department of Chemistry, Texas A&M University, College Station, Texas 77842, United States; orcid.org/0000-0001-9163-7530

Yen-Nan Lin — Department of Chemistry, Texas A&M University, College Station, Texas 77842, United States; College of Medicine, Texas A&M University, Bryan, Texas 77807, United States; ⊙ orcid.org/0000-0001-7118-7771

Rachel A. Letteri – Department of Chemistry, Texas A&M University, College Station, Texas 77842, United States

Lu Su – Department of Chemistry, Texas A&M University, College Station, Texas 77842, United States

Mei Dong — Department of Chemistry, Texas A&M University, College Station, Texas 77842, United States; orcid.org/0000-0002-9862-0296

Fuwu Zhang — Department of Chemistry, Texas A&M University, College Station, Texas 77842, United States; orcid.org/0000-0002-1928-3472

Complete contact information is available at: https://pubs.acs.org/10.1021/acs.nanolett.1c00776

#### Notes

The authors declare the following competing financial interest(s): D.A.H. serves on the Board of Directors for BioVersys AG, Basel, Switzerland.

# ACKNOWLEDGMENTS

This work was supported by the National Science Foundation (CHE-1610311, CHE-2003771, DMREF-1629094) and National Institutes of Health (R01-DK111541, R01-DK126997, and T32-DK007126). We also gratefully acknowledge financial support from the Robert A. Welch Foundation through the W. T. Doherty-Welch Chair in Chemistry (A-0001). Uses of the Texas A&M University Laboratory for Synthetic-Biologic Interactions (LSBI) and the Texas A&M Microscopy and Imaging Center are acknowledged. We also appreciate experimental contributions from Dr. Hansoo Kim for obtaining elemental mapping TEM data. Confocal data were generated on a Zeiss LSM880 Airyscan confocal microscope, which was purchased with support from the Office of Research Infrastructure Programs (ORIP), part of the Office of the Director, National Institutes of Health, under Grant S10-OD021629.

## REFERENCES

- (1) Foxman, B. Urinary Tract Infection Syndromes: Occurrence, Recurrence, Bacteriology, Risk Factors, and Disease Burden. *Infect. Dis. Clin. North Am.* **2014**, 28 (1), 1–13.
- (2) Nielubowicz, G. R.; Mobley, H. L. T. Host-pathogen interactions in urinary tract infection. *Nat. Rev. Urol.* **2010**, *7* (8), 430–441.
- (3) Flores-Mireles, A. L.; Walker, J. N.; Caparon, M.; Hultgren, S. J. Urinary tract infections: epidemiology, mechanisms of infection and treatment options. *Nat. Rev. Microbiol.* **2015**, *13* (5), 269–284.
- (4) Kim, M.; Ashida, H.; Ogawa, M.; Yoshikawa, Y.; Mimuro, H.; Sasakawa, C. Bacterial Interactions with the Host Epithelium. *Cell Host Microbe* **2010**, 8 (1), 20–35.
- (5) Foxman, B. The epidemiology of urinary tract infection. *Nat. Rev. Urol.* **2010**, *7*, 653.
- (6) Chen, Y.-H.; Ko, W.-C.; Hsueh, P.-R. Emerging resistance problems and future perspectives in pharmacotherapy for complicated urinary tract infections. *Expert Opin. Pharmacother.* **2013**, *14* (5), 587–596.
- (7) Asmat, U.; Mumtaz, M. Z.; Malik, A. Rising prevalence of multidrug-resistant uropathogenic bacteria from urinary tract infections in pregnant women. J. Taibah Univ. Medical Sci. 2021, 16 (1), 102–111.
- (8) Durán, N.; Durán, M.; de Jesus, M. B.; Seabra, A. B.; Fávaro, W. J.; Nakazato, G. Silver nanoparticles: A new view on mechanistic aspects on antimicrobial activity. *Nanomedicine* **2016**, *12* (3), 789–790
- (9) Wakshlak, R. B.; Pedahzur, R.; Avnir, D. Antibacterial activity of silver-killed bacteria: the "zombies" effect. *Sci. Rep.* **2015**, *5*, 9555.
- (10) Jung, W. K.; Koo, H. C.; Kim, K. W.; Shin, S.; Kim, S. H.; Park, Y. H. Antibacterial activity and mechanism of action of the silver ion in *Staphylococcus aureus* and *Escherichia coli. Appl. Environ. Microbiol.* **2008**, 74 (7), 2171–2178.
- (11) Silver, S. Bacterial silver resistance: molecular biology and uses and misuses of silver compounds. *FEMS Microbiol. Rev.* **2003**, *27* (2–3), 341–353.
- (12) Qindeel, M.; Barani, M.; Rahdar, A.; Arshad, R.; Cucchiarini, M. Nanomaterials for the Diagnosis and Treatment of Urinary Tract Infections. *Nanomaterials* **2021**, *11* (2), 546.
- (13) Elias, D. R.; Poloukhtine, A.; Popik, V.; Tsourkas, A. Effect of ligand density, receptor density, and nanoparticle size on cell targeting. *Nanomedicine* **2013**, *9* (2), 194–201.

- (14) Gao, H.; Yang, Z.; Zhang, S.; Cao, S.; Shen, S.; Pang, Z.; Jiang, X. Ligand modified nanoparticles increases cell uptake, alters endocytosis and elevates glioma distribution and internalization. *Sci. Rep.* 2013, 3, 2534.
- (15) Zhao, J.; Stenzel, M. H. Entry of nanoparticles into cells: the importance of nanoparticle properties. *Polym. Chem.* **2018**, 9 (3), 259–272.
- (16) Tan, Z.; Jiang, Y.; Ganewatta, M. S.; Kumar, R.; Keith, A.; Twaroski, K.; Pengo, T.; Tolar, J.; Lodge, T. P.; Reineke, T. M. Block Polymer Micelles Enable CRISPR/Cas9 Ribonucleoprotein Delivery: Physicochemical Properties Affect Packaging Mechanisms and Gene Editing Efficiency. *Macromolecules* **2019**, *52* (21), 8197–8206.
- (17) Elsabahy, M.; Song, Y.; Eissa, N. G.; Khan, S.; Hamad, M. A.; Wooley, K. L. Morphologic design of sugar-based polymer nanoparticles for delivery of antidiabetic peptides. *J. Controlled Release* **2021**, 334, 1–10.
- (18) Spirescu, V. A.; Chircov, C.; Grumezescu, A. M.; Andronescu, E. Polymeric Nanoparticles for Antimicrobial Therapies: An up-to-date Overview. *Polymers* **2021**, *13* (5), 724.
- (19) Young, K. D. The Selective Value of Bacterial Shape. *Microbiol. Mol. Biol. Rev.* **2006**, 70 (3), 660–703.
- (20) Martinez, J. J.; Mulvey, M. A.; Schilling, J. D.; Pinkner, J. S.; Hultgren, S. J. Type 1 pilus-mediated bacterial invasion of bladder epithelial cells. *EMBO J.* **2000**, *19* (12), 2803–2812.
- (21) Lin, L. Y.; Tiemann, K. M.; Li, Y.; Pinkner, J. S.; Walker, J. N.; Hultgren, S. J.; Hunstad, D. A.; Wooley, K. L. Synthetic Polymer Nanoparticles Conjugated with FimHA from *E. coli* Pili to Emulate the Bacterial Mode of Epithelial Internalization. *J. Am. Chem. Soc.* **2012**, *134* (9), 3938–41.
- (22) Hannan, T. J.; Totsika, M.; Mansfield, K. J.; Moore, K. H.; Schembri, M. A.; Hultgren, S. J. Host-pathogen checkpoints and population bottlenecks in persistent and intracellular uropathogenic Escherichia coli bladder infection. *FEMS Microbiol. Rev.* **2012**, *36* (3), 616–648.
- (23) Zhang, K.; Rossin, R.; Hagooly, A.; Chen, Z.; Welch, M. J.; Wooley, K. L. Folate-mediated cell uptake of shell-crosslinked spheres and cylinders. *J. Polym. Sci., Part A: Polym. Chem.* **2008**, 46 (22), 7578–7583.
- (24) Sharma, G.; Valenta, D. T.; Altman, Y.; Harvey, S.; Xie, H.; Mitragotri, S.; Smith, J. W. Polymer particle shape independently influences binding and internalization by macrophages. *J. Controlled Release* **2010**, *147* (3), 408–412.
- (25) Ferrag, C.; Li, S.; Jeon, K.; Andoy, N. M.; Sullan, R. M. A.; Mikhaylichenko, S.; Kerman, K. Polyacrylamide hydrogels doped with different shapes of silver nanoparticles: Antibacterial and mechanical properties. *Colloids Surf., B* **2021**, *197*, 111397.
- (26) Bai, S.; Jia, D.; Ma, X.; Liang, M.; Xue, P.; Kang, Y.; Xu, Z. Cylindrical polymer brushes-anisotropic unimolecular micelle drug delivery system for enhancing the effectiveness of chemotherapy. *Bioactive Materials* **2021**, *6* (9), 2894–2904.
- (27) Gratton, S. E. A.; Ropp, P. A.; Pohlhaus, P. D.; Luft, J. C.; Madden, V. J.; Napier, M. E.; DeSimone, J. M. The effect of particle design on cellular internalization pathways. *Proc. Natl. Acad. Sci. U. S. A.* 2008, 105 (33), 11613–11618.
- (28) Liu, X.; Wu, F.; Tian, Y.; Wu, M.; Zhou, Q.; Jiang, S.; Niu, Z. Size Dependent Cellular Uptake of Rod-like Bionanoparticles with Different Aspect Ratios. *Sci. Rep.* **2016**, *6*, 24567.
- (29) Agarwal, R.; Singh, V.; Jurney, P.; Shi, L.; Sreenivasan, S. V.; Roy, K. Mammalian cells preferentially internalize hydrogel nanodiscs over nanorods and use shape-specific uptake mechanisms. *Proc. Natl. Acad. Sci. U. S. A.* **2013**, *110* (43), 17247–17252.
- (30) Decuzzi, P.; Ferrari, M. The adhesive strength of non-spherical particles mediated by specific interactions. *Biomaterials* **2006**, 27 (30), 5307–5314.
- (31) Pitto-Barry, A.; Kirby, N.; Dove, A. P.; O'Reilly, R. K. Expanding the scope of the crystallization-driven self-assembly of polylactide-containing polymers. *Polym. Chem.* **2014**, *5* (4), 1427–1436.

- (32) Song, Y.; Chen, Y.; Su, L.; Li, R.; Letteri, R. A.; Wooley, K. L. Crystallization-driven assembly of fully degradable, natural product-based poly(L-lactide)-*block*-poly( $\alpha$ -D-glucose carbonate)s in aqueous solution. *Polymer* **2017**, *122*, 270–279.
- (33) Song, Y.; Ji, X.; Dong, M.; Li, R.; Lin, Y. N.; Wang, H.; Wooley, K. L. Advancing the Development of Highly-Functionalizable Glucose-Based Polycarbonates by Tuning of the Glass Transition Temperature. *J. Am. Chem. Soc.* **2018**, *140* (47), 16053–16057.
- (34) Gregory, G. L.; Lopez-Vidal, E. M.; Buchard, A. Polymers from sugars: cyclic monomer synthesis, ring-opening polymerisation, material properties and applications. *Chem. Commun.* **2017**, *53* (14), 2198–2217.
- (35) Maiti, S.; Manna, S.; Shen, J.; Esser-Kahn, A. P.; Du, W. Mitigation of Hydrophobicity-Induced Immunotoxicity by Sugar Poly(orthoesters). *J. Am. Chem. Soc.* **2019**, *141* (11), 4510–4514.
- (36) Song, Y.; Yang, X.; Shen, Y.; Dong, M.; Lin, Y.-N.; Hall, M. B.; Wooley, K. L. Invoking Side-Chain Functionality for the Mediation of Regioselectivity during Ring-Opening Polymerization of Glucose Carbonates. *J. Am. Chem. Soc.* **2020**, *142* (40), 16974–16981.
- (37) Dove, A. P. Organic Catalysis for Ring-Opening Polymerization. ACS Macro Lett. 2012, 1 (12), 1409–1412.
- (38) Kamber, N. E.; Jeong, W.; Waymouth, R. M.; Pratt, R. C.; Lohmeijer, B. G.; Hedrick, J. L. Organocatalytic ring-opening polymerization. *Chem. Rev.* **2007**, *107* (12), 5813–40.
- (39) Jewett, J. C.; Bertozzi, C. R. Cu-free click cycloaddition reactions in chemical biology. *Chem. Soc. Rev.* **2010**, 39 (4), 1272–1279.
- (40) Ngo, J. T.; Adams, S. R.; Deerinck, T. J.; Boassa, D.; Rodriguez-Rivera, F.; Palida, S. F.; Bertozzi, C. R.; Ellisman, M. H.; Tsien, R. Y. Click-EM for imaging metabolically tagged nonprotein biomolecules. *Nat. Chem. Biol.* **2016**, *12* (6), 459–465.
- (41) Sun, L.; Petzetakis, N.; Pitto-Barry, A.; Schiller, T. L.; Kirby, N.; Keddie, D. J.; Boyd, B. J.; O'Reilly, R. K.; Dove, A. P. Tuning the Size of Cylindrical Micelles from Poly(L-lactide)-b-poly(acrylic acid) Diblock Copolymers Based on Crystallization-Driven Self-Assembly. *Macromolecules* **2013**, *46* (22), 9074–9082.
- (42) He, Y.; Eloi, J.-C.; Harniman, R. L.; Richardson, R. M.; Whittell, G. R.; Mathers, R. T.; Dove, A. P.; O'Reilly, R. K.; Manners, I. Uniform Biodegradable Fiber-Like Micelles and Block Comicelles via "Living" Crystallization-Driven Self-Assembly of Poly(l-lactide) Block Copolymers: The Importance of Reducing Unimer Self-Nucleation via Hydrogen Bond Disruption. J. Am. Chem. Soc. 2019, 141 (48), 19088–19098.
- (43) Cha, Y.; Jarrett-Wilkins, C.; Rahman, M. A.; Zhu, T.; Sha, Y.; Manners, I.; Tang, C. Crystallization-Driven Self-Assembly of Metallo-Polyelectrolyte Block Copolymers with a Polycaprolactone Core-Forming Segment. ACS Macro Lett. 2019, 8 (7), 835–840.
- (44) Pearce, S.; He, X.; Hsiao, M.-S.; Harniman, R. L.; MacFarlane, L. R.; Manners, I. Uniform, High-Aspect-Ratio, and Patchy 2D Platelets by Living Crystallization-Driven Self-Assembly of Crystallizable Poly(ferrocenyldimethylsilane)-Based Homopolymers with Hydrophilic Charged Termini. *Macromolecules* **2019**, 52 (16), 6068–6079.
- (45) Li, Z.; Zhang, Y.; Wu, L.; Yu, W.; Wilks, T. R.; Dove, A. P.; Ding, H.-m.; O'Reilly, R. K.; Chen, G.; Jiang, M. Glyco-Platelets with Controlled Morphologies via Crystallization-Driven Self-Assembly and Their Shape-Dependent Interplay with Macrophages. *ACS Macro Lett.* **2019**, 8 (5), 596–602.
- (46) Li, R.; Elsabahy, M.; Song, Y.; Wang, H.; Su, L.; Letteri, R. A.; Khan, S.; Heo, G. S.; Sun, G.; Liu, Y.; Wooley, K. L. Functional, Degradable Zwitterionic Polyphosphoesters as Biocompatible Coating Materials for Metal Nanostructures. *Langmuir* **2019**, *35* (5), 1503–1512.
- (47) Elsabahy, M.; Wooley, K. L.; Hendricksen, A.; Oh, K. Multiplexing techniques for measurement of the immunomodulatory effects of particulate materials: Precautions when testing micro- and nano-particles. *Methods* **2019**, *158*, 81–85.
- (48) Elsabahy, M.; Wooley, K. L. Reassessment of nanomaterials immunotoxicity. *Nano Today* **2018**, *20*, 10–12.

- (49) Zhang, P.; Jain, P.; Tsao, C.; Yuan, Z.; Li, W.; Li, B.; Wu, K.; Hung, H.-C.; Lin, X.; Jiang, S. Polypeptides with High Zwitterion Density for Safe and Effective Therapeutics. *Angew. Chem., Int. Ed.* **2018**, *57* (26), 7743–7747.
- (50) Liu, S.; Jiang, S. Zwitterionic polymer-protein conjugates reduce polymer-specific antibody response. *Nano Today* **2016**, *11* (3), 285–291.
- (51) Elkrewi, E.; Randall, C. P.; Ooi, N.; Cottell, J. L.; O'Neill, A. J. Cryptic silver resistance is prevalent and readily activated in certain Gram-negative pathogens. *J. Antimicrob. Chemother.* **2017**, 72 (11), 3043–3046.
- (52) Lim, Y. H.; Tiemann, K. M.; Heo, G. S.; Wagers, P. O.; Rezenom, Y. H.; Zhang, S.; Zhang, F.; Youngs, W. J.; Hunstad, D. A.; Wooley, K. L. Preparation and in Vitro Antimicrobial Activity of Silver-Bearing Degradable Polymeric Nanoparticles of Polyphosphoester-block-Poly(L-lactide). ACS Nano 2015, 9 (2), 1995–2008.
- (53) Li, Y.; Hindi, K.; Watts, K. M.; Taylor, J. B.; Zhang, K.; Li, Z.; Hunstad, D. A.; Cannon, C. L.; Youngs, W. J.; Wooley, K. L. Shell crosslinked nanoparticles carrying silver antimicrobials as therapeutics. *Chem. Commun.* **2010**, *46* (1), 121–123.